# A Pre-screened and Normalized Multiple Endmember Spectral Mixture Analysis for Mapping Impervious Surface Area in Lake Kasumigaura Basin, Japan

Fan YANG, Bunkei MATSUSHITA*, Takehiko FUKUSHIMA

Graduate School of Life and Environmental Science, University of Tsukuba

1-1-1, Tennoudai, Tsukuba, Ibaraki. 305-8572, Japan

* Corresponding Author

Tel: +81-29-853-7190

Fax: +81-29-853-7190

E-mail: mbunkei@sakura.cc.tsukuba.ac.jp

# A Pre-screened and Normalized Multiple Endmember Spectral Mixture Analysis for Mapping Impervious Surface Area in Lake Kasumigaura Basin, Japan


## Abstract

The impervious surface area (ISA) has emerged not only as an indicator of the degree of urbanization, but also as a major indicator of environmental quality for drainage basin management. However, since almost all of the methods for estimating ISA have been developed for urban environments, it is questionable whether these methods can be successfully applied to drainage basins, such as those found in Japan, which usually have more complicated vegetation components (e.g. paddy field, plowed field and dense forest). This paper presents a pre-screened and normalized multiple endmember spectral mixture analysis (PNMESMA) method, which includes a new endmember selection strategy and an integration of the Normalized Spectral Mixture Analysis (NSMA) and Multiple Endmember Spectral Mixture Analysis (MESMA), for estimating the ISA fraction in Lake Kasumigaura Basin, Japan. This new proposed method is superior to the previous methods in that the estimation error of the proposed method is much smaller than the previous SMA- or NSMA-based methods for drainage basin environments. The overall root mean square error was reduced to 5.2%, and no obvious underestimation or overestimation occurred for high or low ISA areas. Through the assessment of environmental quality in Lake Kasumigaura Basin using the ISA fraction, the results showed that the basin has been in the impacted category since 1987, and that in the two decades since, the environmental quality has continued to decline. If this decline continues, then Lake Kasumigaura Basin will fall into the degraded category by 2017.



**Key words**: Impervious Surface Area, Spectral Mixture Analysis, Endmember Selection, Lake Kasumigaura Basin

## 1. Introduction

The Impervious Surface Area (ISA) is defined as an area consisting of constructed surfaces (roofs, roads, parking lots, driveways, sidewalks, and other surfaces) which prevent water from infiltrating into the soil. The ISA has emerged not only as an indicator of the degree of urbanization, but as a major indicator of environmental quality for drainage basin management (Arnold and Gibbons, 1996). Previous studies pointed out that the increase of ISA has changed the hydrological character (White and Greer, 2006; Xian et al., 2007) and heat balance (Kato and Yamaguchi, 2007; Yuan and Bauer, 2007) of drainage basins, put environmental pressure on the aquatic ecosystem (Alberti et al., 2007), and had other detrimental effects. A widely accepted scale for the impact of the ISA on drainage basins are: stressed if they contain 1-10% ISA, impacted if they contain 10%-25% ISA and degraded if they contain more than 25% ISA (Arnold and Gibbons, 1996; Elvidge et al., 2007; Schueler, 1994). Therefore, it is essential to accurately estimate the ISA for effective management of drainage basins.

Remote sensing techniques, which have the inherent ability to provide spatial and temporal information about the Earth surface, may be the only viable way to effectively monitor large scale land use/cover change such as that around a drainage basin. However, accurately estimating the ISA from satellite data is still challenging because the ISA always results in spectral heterogeneity at scales comparable to sensor resolution, which limits the utility of conventional hard classification methods (Small, 2001). To solve the problem of spectral heterogeneity, a vegetation-impervious surface-soil model (V-I-S) was proposed for parameterizing the biophysical composition of urban environments (Ridd, 1995). In this model, a given pixel can be modeled by the fractions of vegetation, impervious surface and soil, based on spectral mixture analysis (SMA). On the basis of SMA and V-I-S models, many studies in which the ISA was estimated have been conducted in urban areas (Phinn et al., 2002; Powell et al., 2007; Rashed et al., 2005; Small and Lu, 2006; Wu and

Murray, 2003).

The success of the application of SMA and V-I-S models for accurately estimating ISA fractions depends on the selection of the endmember components (Dennison and Roberts, 2003a; Dennison and Roberts, 2003b). According to the V-I-S model, three endmembers, vegetation, impervious surface, and soil can be selected for the SMA. However, due to the complexity of spectral reflectance for ISA, more endmembers are required to explain more spectral variation, thereby increasing model fitness. For example, some applications in urban areas generally sub-classify impervious surfaces into two different endmembers, i.e. low albedo (e.g. asphalt) and high albedo (e.g. concrete) (Lu and Weng, 2006; Small, 2001; Wu and Murray, 2003). Vegetation and soil also show spectral complexities, with similar spectral shapes but different spectral magnitudes because of different leaf characteristics, canopy geometry, and leaf angle distributions for vegetation, and soil composition, grain size, and water content for soil (Matsushita and Fukushima, 2009; Wu, 2004; Dennison and Roberts, 2003a). However, too many endmembers make the mixture model not only sensitive to endmember selection, but also make it impossible to apply the model to multispectral imagery and thus potentially make the model inapplicable to most cases (Matsushita and Fukushima, 2009; Sabol et al., 1992; Wu and Murray, 2003). Wu (2004) proposed a normalized spectral mixture analysis (NSMA) to address the problems associated with spectral complexity (e.g. brightness variation and shade effect within each endmember). Lu and Weng (2006) developed another method by using the land surface temperature to remove non-impervious surfaces from the low albedo and high albedo estimations, which improved the accuracy of ISA estimation without any addition of endmember numbers. Powell et al. (2007) reported that multiple endmember spectral mixture analysis (MESMA), which allows the number and type of endmembers to vary from pixel to pixel, can also be used to address the problem of spectral variability. However, almost all of the SMA- or NSMA-based methods for estimating ISA have been developed for urban environments. Therefore,

it is questionable whether these methods can also be successfully applied to an Asian drainage basin in which each endmember, particularly those for different vegetation species, has more complicated characteristics (Song, 2004; Song, 2005).

The objectives of this study are: 1) to develop a new NSMA-based method that can accurately estimate ISA in a drainage basin with the Lake Kasumigaura Basin as a case study; 2) to show the performance of the proposed method by comparing it with several previous methods, and 3) to assess the environmental quality of the Lake Kasumigaura Basin and explore its twenty-year changes using the ISA as an indicator. In the method development process, two main problems were considered. One is the vegetation endmember selection, which takes into account the vegetation diversity; the other is to overcome the flaws existing in the original SMA- or NSMA-based methods, which lead to underestimation in high ISA areas or overestimation in low ISA areas.

## 2. Study Area

The Lake Kasumigaura Basin is located in the eastern part of the Kanto Plain of Japan, and covers an area of about 2157 $km^2$ (Fig.1). The population of the Lake Kasumigaura Basin was approximately 1 million in 2000. With a surface area of 220 $km^2$ and an average depth of 4m, the lake is the second largest in Japan. The climate of the area is similar to other regions on the Pacific side of Japan with an annual average air temperature of about 14 ℃ and an annual precipitation of 1250 mm.

(Please insert Fig.1 here)

The dominant landscapes in the Lake Kasumigaura Basin are paddy fields (25.8%), forests (22.7%), plowed fields (21.2%), and water (10.6%) (Matsushita et al. 2006). The traditional industries in this area are agriculture, livestock management, and fishery production. However, many new industrial plants have been constructed, and industrial shipments from the area continue to rise every year. Since the study area is only 60 km from Tokyo, there has been a rapid rise in the number

of residents, recreational facilities, and resort areas in recent years, which has caused rapid changes in the landscape structure in the past decades. From 1979 to 1996, human-modified landscapes, such as artificial fields and golf courses, increased rapidly, while forests and croplands rapidly decreased (Fukushima et al., 2007). Increased patch (landscape element) numbers, Shannon's diversity, and decreased mean patch area have indicated that the Lake Kasumigaura Basin has become more fragmented and heterogeneous (Matsushita et al., 2006). With the completion of a new railroad linking Tsukuba and the Akihabara area of Tokyo in 2005, this trend is likely to persist as the population in the Lake Kasumigaura Basin continues to increase.

## 3. Image pre-processing

Four scenes of cloud-free or little cloud contaminated Landsat-5 TM images (Row 107/Path 35) were collected for the Lake Kasumigaura Basin. These images were acquired on July 24, 1987, July 19, 1999, July 11, 2000, and August 16, 2007. All images were geometrically corrected to UTM (Universal Transverse Mercator) projection (Zone 54N; Spheroid: GRS1980; Datum: JGD2000). The GSI Digital Map 25000 (Geographical Survey Institute, Japan, 1:25000, published in 2002) was used as the reference image for geometric correction. A first order polynomial model was applied for the rectification with the nearest neighbor resampling method. The root mean square errors were less than 0.1 pixels (3m) for all satellite images.

Relative radiometric normalization by automatic scattergram-controlled regression (ASCR) was carried out to compensate for the radiometric divergence present in images acquired under different illumination, atmospheric, or sensor conditions (Elvidge et al., 1995; Yuan and Elvidge, 1996). The image collected on July 24, 1987 was set as a reference image because it was cloud-free and taken under a good sensor condition. After the relative radiometric normalization, the rescaling gain, bias (Chander et al., 2007) and parameters (Chander and Markham, 2003) for the image acquired on July 24, 1987 were applied to all images to convert digital numbers (DNs) to top-of-the-atmosphere

(TOA) reflectance.

Since the images collected on July 19, 1999 and July 11, 2000 contained some cloud coverage in the study area, a cloud mask was first made for the image acquired on July 11, 2000, and then the clear corresponding pixels in the image acquired on July 19, 1999 were used to replace the clouded pixels in the image acquired on July 11, 2000. Finally, the images acquired on July 24, 1987 and August 16, 2007, together with the composited image mainly based on the image acquired on July 11, 2000, were used to investigate ISA distribution in 1987, 2000 and 2007. A water mask was made by the unsupervised classification method (Wu and Murray, 2003), and water pixels in the study area were then removed using this water mask before the ISA estimation.

## 4. Development of a new NSMA-based method for estimating ISA in a drainage basin

### *4.1 Spectral mixture analysis (SMA) and Normalized Spectral Mixture analysis (NSMA)*

A linear spectral mixture analysis model was adopted in this study. For a given pixel, the reflectance for each band b ($R_b$) in the Landsat-5 TM image can be written as:

$$R_b = \sum_{j=1}^{N} f_j R_{j,b} + e_b \tag{1}$$

$$\sum_{j=1}^{N} f_j = 1,\ f_j \geq 0 \tag{2}$$

where N is the number of endmembers (i.e. spectrally 'pure' materials), $f_j$ is the fraction of endmember j, $R_{j,b}$ is the reflectance of endmember j in band b, and $e_b$ is the unmodeled residual indicating the disagreement between the measured and modeled spectra in band b. The fraction of each endmember can be obtained using the least-squares method.

The endmembers were selected from the 1987 image based on the principal component analysis (PCA) method. The PCA method can guide image endmember selection because it puts almost 90% of the variances on the first two or three components and minimizes the influence of band to band correlation (Smith et al., 1985). In this study, the first three principal components (PCs) can explain

about 98.48% of the variances contained in six Landsat-5 TM bands (excluding the thermal band). From three feature space representations (PC1 vs PC2, PC1 vs PC3 and PC2 vs PC3) and their associated interpretations based on the reflectance data, five endmembers (vegetation A, vegetation B, high albedo, low albedo and soil) can be identified (Figs. 2a-2c). Note that the two vegetation endmembers found in the study area are different from the previous results reported in urban areas (e.g. Lu and Weng, 2006; Wu and Murray, 2003; only one vegetation endmember was found in those study areas). The vegetation A pixels were widely found in farmlands (paddy fields and plowed fields) and the vegetation B pixels were found in the forested areas of Mt. Tsukuba and shaded vegetation in urban areas. The high and low albedo pixels were almost all distributed in the urban area and highways (e.g. concrete, asphalt). The soil pixels were mainly found in the harvested fields or fallow land. The extreme pixel clusters which bound almost all other pixels in the feature spaces (Figs. 2a-2c) were delineated as endmembers. The averaged reflectance spectra of these extreme pixel clusters for the five endmembers are shown in Fig.2d.

(Please insert Fig.2 here)

Previous studies suggested that about three to four endmembers are appropriate for simple linear mixture models in the Landsat-5 TM application (Lu and Weng, 2006; Powell et al., 2007; Wu, 2004; Wu and Murray, 2003). Wu (2004) reported that the NSMA method was effective for reducing the brightness variation and shade effect within each endmember and thus could reduce the number of endmembers. He compared the spectral variations of the V-I-S components and their normalized spectra among three different brightness cases (i.e. dark, medium, and bright), and found that significant spectral variation due to brightness differences existing in the original spectra was largely reduced in the normalized spectra. This is because the spectra for each V-I-S component show significant brightness differences, but have the similar spectral shape. Therefore, it is possible to highlight the shape information while minimizing the effects of absolute reflectance values (e.g.

shade effect) through a normalization method, thus allowing a single endmember to represent each component (Wu, 2004).

In the NSMA, the normalized reflectance spectra of each pixel and endmember were used instead of the reflectance spectra in the SMA model. The normalized reflectance for band b in a pixel ($\overline{R_b}$) can be written as:

$$\overline{R_b} = \frac{R_b}{\mu} \tag{3}$$

$$\mu = \frac{1}{M}\sum_{b=1}^{M} R_b \tag{4}$$

where μ is the average reflectance for all bands of that pixel, M is the total number of bands (6 for Landsat-5 TM image), and $R_b$ is the reflectance for band b.

Fig. 3 shows the feature space representations of the first three PCs for the normalized TOA reflectance image of 1987. It shows that vegetation A and vegetation B still could not be integrated as one vegetation endmember in our study area, although Wu (2004) successfully used a single vegetation endmember to represent the vegetation component in his study area through the normalization method. Therefore, it is essential to propose a new strategy (described in Section 4.2) for selecting appropriate endmembers (especially for selecting a single appropriate endmember for vegetation) in order to successfully apply SMA or NSMA in the Lake Kasumigaura Basin.

(Please insert Fig. 3 here)

*4.2 New strategy for endmember selection*

According to the above results, a new strategy was designed for endmember selection:

First, for selecting a vegetation endmember, two indices, i.e. the normalized differences vegetation index (NDVI) and the reflectance at red band ($R_{red}$), were used to extract pure vegetation pixels from the study area. In this study, from the result of endmember selection based on PCA (Fig.2d), it was shown that the NDVI values of both vegetation endmembers A and B were larger

than 0.5. Therefore, the NDVI threshold of 0.5 was used as one condition for extracting pure vegetation pixels. This NDVI value is similar to previous studies, such as 0.46 in Song (2005) and 0.4 in (Nemani and Running, 1997). However, a pixel can still be considered to contain a small sub-pixel non-vegetation fraction even if the pixel has a NDVI value larger than 0.5 (e.g. mixture of the vegetation A and low/high albedo). Consequently, to definitively extract the pure vegetation pixels, another condition, that $R_{red}$ should be lower than 0.07, was added. This is because the addition of a non-vegetation component in a given pixel will reduce the content of chlorophyll-a in the pixel, and thus make $R_{red}$ increase. The threshold of 0.07 for $R_{red}$ was obtained from vegetation endmember A (bright vegetation with an NDVI value of 0.75) shown in Fig. 2d. Based on these two conditions, the pure vegetation pixels were extracted from the reflectance images. The averaged spectra of these extracted pure vegetation pixels were used as the vegetation endmember for the SMA- or NSMA-based (after normalization) methods in the latter analysis.

Second, the endmembers for low albedo, high albedo, and soil were selected from the first three PCs of the original image (Figs.2a-2c). The three selected endmember spectra are shown in Fig. 2d. It was found that the endmember pixels selected from the feature space representations of the original image (Figs. 2a-2c) were different from those selected from the feature space representations of the normalized reflectance image (Figs. 3a-3c based on Wu 2004). Therefore, only the endmember pixels selected from the feature space representations of the reflectance image were used in this study to make the same endmembers that can be used in all of the different SMA- or NSMA-based methods for comparisons.

Finally, the four selected endmembers based on the above results were normalized using equations (3) and (4) for the application of the NSMA-based method (Fig. 4). This is because the normalized transformation can reduce the brightness variation within similar pixels, and thus can reduce the estimation errors due to the limited endmember selection. In addition, the normalized

transformation can remove the effect of shade, which cannot be considered a biophysical composition but a factor adversely influencing modeling results (Wu, 2004). The reflectance spectra shown in Fig. 4 are the final endmembers used in the NSMA-based methods in this study.

(Please insert Fig.4 here)

*4.3 New algorithm for ISA estimation*

A flowchart of the new algorithm for estimating the ISA fraction is shown in Fig.5. There are three major steps in the algorithm.

First, the pure vegetation pixels were extracted based on the two thresholds of NDVI and $R_{red}$ described above, and then directly set as a vegetation fraction of 100% (ISA=0%) before the NSMA application. There are two reasons why the pure vegetation pixels were extracted based on these thresholds. One is that the complexity of spectral reflectance in a drainage basin is more significant than that in an urban area because there are more vegetation species in the drainage basin, and thus using a normalized reflectance image cannot completely remove the brightness variation within the vegetation endmembers (e.g., results shown in Fig. 3). The other is that the drainage basin always includes a large number of pure vegetation pixels, and applying the traditional SMA- or NSMA-based method to these pure vegetation pixels will still result in large errors of ISA estimation (overestimation in low ISA).

Second, similar with the MESMA, all endmember combinations (a total of 15 combinations in this study, i.e. four combinations for 1-endmember models, six combinations for 2-endmember models, four combinations for 3-endmember models, and one combination for the 4-endmember model) were applied to the NSMA model for every remaining pixel in the image; the endmember combination that resulted in all positive endmember fractions and the smallest residual $e_b$ was selected as the optimal combination for each remaining pixel, and the endmember fractions estimated from the optimal endmember combination were considered to be the final result for each

remaining pixel (Powell et al., 2007; Roberts et al., 1998). This is because that any remaining pixel is probably composed of one, two, three, or four endmembers in a drainage basin. If an endmember combination (e.g. four endmembers: vegetation, high albedo, low albedo, and soil) is used to estimate a pixel with different endmember components (e.g. a pixel in which only two endmembers, vegetation and soil, are contained), a larger estimation error will be obtained due to the use of an unsuitable endmember combination. The technique of MESMA allows the number and type of endmembers to be varied from pixel to pixel, and thus can address this problem (Sabol et al., 1992; Roberts et al., 1998; Powell et al., 2007).

Finally, the ISA fraction was calculated as the sum of the low albedo and high albedo fractions because the adverse effects (e.g. water, shade, cloud) on the estimations of low albedo and high albedo fractions were removed or reduced in the previous steps.

According to the above descriptions (Sections 4.2 and 4.3), this new NSMA-based method was named the Pre-screened and Normalized Multiple Endmember Spectral Mixture Analysis (PNMESMA).

(Please insert Fig.5 here)

## 5. Four previous SMA- or NSMA-based methods for comparison

The results of using four previous SMA- or NSMA-based methods were compared with the PNMESMA method described in section 4.The first is the 4-endmember SMA model (method 1 in Table 1). In this method, the vegetation endmember was also obtained from the extracted pure vegetation pixels based on NDVI and $R_{red}$, and the other three endmembers (i.e. high albedo, low albedo and soil) were selected from feature spaces representations of the first three PCA of the reflectance image (Fig.2).

The second SMA-based method is that proposed by Lu and Weng (2006), which is based on the integrations of fractions images from linear spectral mixture analysis and the land surface

temperature (LST) (method 2 in Table 1). This method can remove non-ISA (e.g. shaded vegetation) from low- and high-albedo fraction images and thus improve the accuracy of the ISA estimation. In this method, it is assumed that if the pixel values in the LST image are less than or equal to a threshold $T_0$, the pixels in the low-albedo and high-albedo fraction images would be assigned to zero, because these pixels are identified as shaded vegetation or water (in other words, vegetation and water possess lower land surface temperature values than built-up lands). If the pixel values in the LST image are not less than or equal to a threshold $T_0$, then the pixel values in the low-albedo and high-albedo fraction images would be kept to calculate the ISA fraction (Lu and Weng, 2006). Another assumption of using a threshold in a soil fraction image to remove the dry soils from high-albedo was not used in this study, because there was little dry soil in the study area. The endmember selection was the same as the first method.

The third method is the NSMA method (Wu, 2004) (method 3 in Table 1). Since we found that the endmember pixels selected from the feature space representations of the original image (Figs. 2a-2c) were different from those selected from the feature space representations of the normalized reflectance image (Figs. 3a-3c based on Wu 2004), the normalized reflectance spectra in Fig.4 (the endmember pixels selected from Figs. 2a-2c) were used as the endmembers for the NSMA method for a fair comparison, instead of using endmembers directly selected from Figs. 3a-3c.

The fourth method is the MESMA (Roberts et al., 1998; Powell et al., 2007) (method 4 in Table 1). Different from the original application of MESMA, the NSMA was used instead of SMA in this comparison. Three vegetation endmembers (using the vegetation pixels A and B obtained from Fig. 2 and whole pure vegetation pixels obtained through two thresholds of NDVI and $R_{red}$) and three non-vegetation endmembers (low albedo, high albedo, and soil endmembers obtained from Fig. 4) were used to first build a simple endmember library. Then, a total of 31 NSMA models based on all combinations of library endmembers were applied to every pixel in the image, and the 'best fit'

model was selected for each pixel. The endmember combinations followed the rules suggested by Powell et al. (2007) but without the use of a shade endmember because the NSMA was used in this study.

(Please insert Table 1 here)

In order to compare the accuracy of the ISA estimations among the different methods, a widely used method for developing validation data was applied: extracting the ISA fraction from digital orthophotos (Lu and Weng, 2006; Powell et al., 2007; Wu, 2004; Wu and Murray, 2003; Yuan and Bauer, 2007). The aerial photographs acquired in 1986, 1994, and 2005 (GSI, Japan) were utilized as the ground reference for assessing model accuracy. For each period, three aerial photographs taken in urban areas (Tsukuba City and Tsuchiura City), a rural area (Tamazukuri District) and a mountainous area (Makabe District) were chosen to represent the high, medium, and low ISA fraction, respectively (see Fig. 1). All aerial photographs were geometrically corrected using GSI Digital Map 25000, and the geometric errors are within 1 m. As in Wu (2004), a 3×3 sampling unit (90m × 90m) was utilized to reduce the impact of geometric errors associated with the Landsat-5 TM images and aerial photographs. Since only the aerial photographs taken in 2005 are in color and have finer spatial resolution (0.5m), the actual ISA fractions interpreted from these aerial photographs are more accurate than those from the monochromatic aerial photographs taken in 1986 and 1994. Therefore, only the aerial photographs taken in 2005 were used to assess the ISA estimation accuracies in this study. To use one period of the aerial photographs for assessing the ISA estimation accuracies from three periods of Landsat-5 TM images, a total of 138 random samples without land use/cover change among the three periods were selected by checking both the reflectance spectra of the three TM images and the corresponding aerial photographs taken in 1986, 1994, and 2005. For each sample, the corresponding actual ISA fraction was calculated by visually interpreting the aerial photographs in ArcGIS 9.2. The root mean square error (RMSE) was employed to assess the ISA

estimation accuracy for different methods, which were defined as:

$$RMSE = \sqrt{\frac{\sum_{i=1}^{N} (ISA_{pred,i} - ISA_{actual,i})^2}{N}} \quad (5)$$

where N is the number of validation samples (56 samples for ISA between 0-20%, 28 samples for ISA between 20-40%, 31 samples for ISA between 40-60%, 14 samples for ISA between 60-80%, and 9 samples for ISA between 80-100%). $ISA_{pred,i}$ and $ISA_{actual,i}$ are the predicted and actual ISA fractions for the sample *i*, respectively.

## 6. Results and Discussion

### 6.1 Comparison between the proposed method and previous methods

Fig. 6 shows the comparisons of the ISA estimation accuracy among five SMA- or NSMA-based models. The results shown in Figs. 6a and 6b indicate that the 4-endmember SMA model has large overestimation in the low ISA areas (RMSE=0.129 for ISA between 0-40%) and underestimation in the medium and high ISA areas (RMSE=0.095 for ISA between 40-100%), with an overall RMSE of 0.117 for all samples (also see method 1 in Table 1). The overestimation is mainly due to the complexity of the vegetation reflectance spectra, which resulted from vegetation diversity or shade effects in the study area. For example, if the 4-endmember SMA model was used for a pure vegetation pixel, the differences of reflectance spectra between the vegetation endmember and vegetation in the pixel would result in an overestimation of ISA fraction. The underestimation in the medium and high ISA areas is mainly due to the confusions between shaded non-ISA surfaces and low-albedo surfaces (Lu and Weng, 2006; Wu, 2004).

The results shown in Figs. 6c and 6d suggest that the SMA-based model developed by Lu and Weng (2006) improved the ISA estimation accuracy (overall RMSE =0.091) through the use of LST images, especially in low ISA areas (RMSE =0.079 for ISA between 0-40%, method 2 in Table 1).

However, the underestimations in medium and high ISA areas were not improved (RMSE =0.107 for ISA between 40-100%, method 2 in Table 1). This is probably because the relatively lower spatial resolution of the Landsat-5 TM thermal band smoothed the boundaries between ISA and the other cover types (Lu and Weng, 2006). Figures 6e and 6f show that the NSMA method can slightly improve the ISA estimation accuracy compared with the 4-endmember SMA method (with an overall RMSE of 0.114). However, the overestimation in the low ISA areas (RMSE=0.130 for ISA between 0-40%) and underestimation in the medium and high ISA areas (RMSE=0.081 for ISA between 40-100%) cannot be solved (method 3 in Table 1).

Figures 6g and 6h show that although only a small number of endmembers were contained in the endmember library, the MESMA method still improved the ISA estimation accuracy (overall RMSE =0.098) through varying the number and type of endmembers from pixels to pixel, especially in the medium and high ISA areas (RMSE=0.069 for ISA between 40-100%, method 4 in Table 1). However, the overestimations in low ISA areas have not been improved because a limited number of endmembers were available in this study (RMSE =0.105 for ISA between 0-40%, method 4 in Table 1). If a sufficient number of spectra could be collected to adequately represent the spectral variation of the material on the ground, the MESMA method promises to give an accurate ISA estimation. Even if it does give an accurate ISA estimation, building a sufficient spectral library and the computational efficiency of the MESMA are still two particular challenges (Powell et al., 2007).

In comparison to the four methods above, the PNMESMA method has a promising accuracy in estimating ISA for the whole study area (Figs. 6i and 6j). The overall RMSE was reduced to 0.052, and no obvious underestimation and overestimation were found for all samples (RMSE =0.045 for ISA between 0-40%; RMSE=0.060 for ISA between 40-100%, method 5 in Table 1). The coefficient of determination ($R^2$=0.96) was also improved compared with the previous methods ($R^2$=0.81-0.91). In this study, two improvements were carried out to overcome the limitations in the previous SMA-

or NSMA-based methods. To further demonstrate the role of each improvement, the results with only one improvement are also shown in Fig.7 for comparison.

(Please insert Fig.6 here)

(Please insert Fig.7 here)

The first improvement was the use of two indices (NDVI and $R_{red}$) to extract pure vegetation pixels before the application of the NSMA, and the reflectance spectra of all extracted pure vegetation pixels were averaged and normalized to obtain the vegetation endmember (method 6 in Table 1). The ISA fractions of these extracted pixels were directly set to 0%. This improvement can avoid the effects of spectral complexity within vegetation endmembers when applying the SMA or NSMA, thus giving an accurate ISA estimation in less developed areas, like mountainous or agricultural areas (RMSE=0.056 for ISA between 0-40%, method 6 in Table 1 and Figs 7a and 7b), while this improvement cannot overcome the underestimation in high ISA areas very well (RMSE=0.098 for ISA between 40-100%).

The second improvement is applying the MESMA method but using NSMA instead of SMA in the new method. For this, a total of 15 endmember combinations were tested for all remaining pixels (excluding the pure vegetation pixels), and the results obtained from the endmember combination with all endmember fractions larger or equal to zero and the smallest residual were kept as the final ISA estimation results (method 7 in Table 1). This improvement allowed us to choose the optimal endmember combination for a given pixel, thus yielding more accurate ISA estimations, especially in medium and high ISA fraction areas (RMSE=0.054 for ISA between 40-100%, method 7 in Table 1 and Figs. 7c and 7d). However, this improvement was not sufficient to solve the overestimation problem in low ISA areas (RMSE=0.163 for ISA between 0-40%).

Accordingly, integrating the two improvements described above, the new proposed PNMESMA method successfully overcame the flaws of the original SMA- or NSMA-based method. In addition,

compared with the original application of MESMA, through the integration of the two improvements, the PNMESMA method reduced not only the number of pixels that the MESMA was applied to (because the pure vegetation pixels were pre-screened) but also the number of endmembers needed, thus decreasing potential models and increasing the computational efficiency. Therefore, the PNMESMA method can be used to estimate the ISA distribution for a large scale basin such as the Lake Kasumigaura Basin.

### 6.2 Twenty-year change of ISA in the Lake Kasumigaura Basin

The ISA distribution maps for the Lake Kasumigaura Basin (Fig. 8) were obtained from the Landsat TM-5 images based on the new SMA-based model described in section 4. The ISA fraction images are consistent with the urban distribution in the study area, such as the high ISA in Tsukuba City, Tsuchiura City, Ishioka City and so on. In contrast, mountainous and agricultural areas show very low ISA. Table 2 summarizes the ISA fractions in different river basins (sub-basins, Fig. 9) and the whole Kasumigaura Basin for 1987, 2000, and 2007. To further explore the trend in the study area, the change rates and predicted results after five or ten years based on the 20-year change rate (Rate 87-07 in Table 2) are also listed in Table 2. During the periods 1987-2000 and 2000-2007, the ISA fraction increased from 19.9% to 21.8% and from 21.8% to 23.7%, respectively, for the whole Lake Kasumigaura Basin. This result indicates that the whole Lake Kasumigaura Basin had already fallen in the impacted category (10-25% ISA cover) in 1987, and the rank has been continuously sliding towards the degraded category in the two decades since. In addition, the rate of the ISA fraction increase has further accelerated from 0.15%/year in the period from 1987-2000 to 0.27%/year in the 2000-2007 period.

(Please insert Fig. 8 here)

(Please insert Table 2 here)

(Please insert Fig. 9 here)

For the analysis at the sub-basin scale, the results show that all sub-basins have ISA fractions larger than 10%; seven sub-basins (303.4 $km^2$, accounting for 16% of the total basin) fell in the degraded category and the remaining sixteen sub-basins fell in the impacted category in 1987. The sub-basins with more than 25% of their areas covered by ISA are almost all crossed by the Joban highway linking Tokyo and Sendai, except for the Hokota River Basin. After 1987, the number of sub-basins falling into the degraded category increased to eight in 2000 and nine in 2007, accounting for 18% (328.4 $km^2$) and 25% (471.4 $km^2$) of the total study area, respectively. The change rates for almost all of the sub-basins (except for the Koise River Basin, Hishiki River Basin, and Mae River Basin) showed increasing trends during the 1987-2007 periods. However, several sub-basins showed negative change rates in Table 2. After checking the pixels with the obviously reduced ISA in the two periods, it was found that these pixels almost all fall in the land use type consisting of golf courses. This result indicates that the ISA reduction is probably due to the construction of golf courses before the periods and the recovery of vegetation during the periods.

Overall, the Lake Kasumigaura Basin showed a high ISA fraction level early in 1987, and the ISA fraction has increased continuously since the 1980s, when Japan experienced very rapid economic development. Since the study area is only 60 km from Tokyo, the construction of the Joban highway which links Tokyo to the study area has led to a rapid rise in the number of residents, recreational facilities, and resort areas in the Lake Kasumigaura Basin within this period (Matsushita et al., 2006). Although the economic bubble burst in the early 1990s, we still found that the ISA fraction continued to increase at an even faster pace from 2000 to 2007, a period during which the rate of increase was about two times that of the 1987-2000 period. These results suggest that if this increasing trend continues, Lake Kasumigaura Basin will fall in the degraded category in ten years (i.e. in 2017), and 56% (1041.3 $km^2$) or 63% (1171 $km^2$) of the total study area will suffer the adverse effects of ISA after five years or ten years, respectively. Therefore, appropriate assessment

techniques such as accurate estimation of the ISA fraction will provide critical information to policymakers for efficient development and management of the drainage basin as well as for sustainable growth in this region.

## 7. Conclusions

This paper presented a pre-screened and normalized multiple endmember spectral mixture analysis (PNMESMA) method for estimating the ISA fraction in a drainage basin. The new proposed method possesses two improvements: (1) extracting the pure vegetation pixels before the application of NSMA by the uses of NDVI and $R_{red}$; the extracted pure vegetation pixels were then used to obtain the vegetation endmembers; (2) applying the MESMA method but using NSMA instead of SMA for every remaining pixel. The results show that the proposed method improved the ISA estimation accuracy compared with the previous SMA- or NSMA-based methods. In the case of the Lake Kasumigaura Basin, the overall RMSE was reduced to 5.2%, and there was no obvious underestimation or overestimation for high or low ISA areas.

The environmental quality of Lake Kasumigaura Basin and its twenty-year change were assessed by using the ISA fraction as an indicator. The results show that the Lake Kasumigaura Basin had already fallen into the impacted category in 1987, and has been continuously sliding towards the degraded category in the two decades since. If this increasing trend continues, more than half of Lake Kasumigaura Basin will fall in the degraded category in ten years (i.e. in 2017).

More study is required to explore the performance of this new NSMA-based method in other drainage basins.

## Acknowledgement

The authors would like to thank two anonymous reviewers for their helpful comments and suggestions.

*Reference*

Alberti, M. Booth, D., Hill, K., Coburn, B., Avolio, C., Coe, S., Spirandelli., D., 2007. The impact of urban patterns on aquatic ecosystems: An empirical analysis in Puget lowland sub-basins. Landscape and Urban Planning 80(4), 345-361.

Arnold, C.L., Gibbons, C.J., 1996. Impervious Surface Coverage: the Emergence of a Key Environmental Indicator. Journal of the American Planning Association 62(2), 243-258.

Chander, G., Markham, B., 2003. Revised Landsat-5 TM Radiometric Calibration Procedures and Postcalibration Dynamic Ranges. IEEE Transactions on Geoscience and Remote Sensing 41(11), 2674-2677.

Chander, G., Markham, B.L., Barsi, J.A., 2007. Revised Landsat-5 Thematic Mapper Radiometric Calibration. IEEE Geoscience and Remote Sensing Letters 4(3), 490-494.

Dennison, P.E., Roberts, D.A., 2003a. The effects of vegetation phenology on endmember selection and species mapping in southern California chaparral. Remote Sensing of Environment 87(2-3), 295-309.

Dennison, P.E., Roberts, D.A., 2003b. Endmember selection for multiple endmember spectral mixture analysis using endmember average RMSE. Remote Sensing of Environment 87(2-3), 123-135.

Elvidge, C.D., Tuttle, B.T., Sutton, P.C., Baugh, K.E., Howard, A.T., Milesi, C., Bhaduri, B., Nemani, R., 2007. Global Distribution and Density of Constructed Impervious Surfaces. Sensors 7(9), 1962-1979.

Elvidge, C.D., Yuan, D., Weerackoon, R.D., Lunetta, R.S., 1995. Relative Radiometric Normalization of Landsat Multispectral Scanner (MSS) Data Using an Automatic Scattergram-Controlled Regression. Photogrammetric Engineering & Remote Sensing 61(10), 1255-1260.

Fukushima, T., Takahashi, M., Matsushita, B., Okanishi, Y., 2007. Land use/cover change and its drivers: a case in the watershed of Lake Kasumigaura, Japan. Landscape and Ecological Engineering 3(1), 21-31.

Kato, S., Yamaguchi, Y., 2007. Estimation of storage heat flux in an urban area using ASTER data. Remote Sensing of Environment 110(1), 1-17.

Lu, D., Weng, Q., 2006. Use of impervious surface in urban land-use classification. Remote Sensing of Environment 102(1-2), 146-160.

Matsushita, B., Fukushima, T., 2009. Methods for retrieving hydrologically significant surface parameters from remote sensing: a review for applications to east Asia region. Hydrological Processes 23(4), 524-533.

Matsushita, B., Xu, M., Fukushima, T., 2006. Characterizing the changes in landscape structure in the Lake Kasumigaura Basin, Japan using a high-quality GIS dataset. Landscape and Urban Planning 78(3), 241-250.

Nemani, R., Running, S., 1997. Land Cover Characterization Using Multitemporal Red, Near-IR, and Thermal-IR Data from NOAA/AVHRR. Ecological Application 7(1), 79-90.

Phinn, S., Stanford, M., Scarth, P., Murray, A.T., Shyy, P.T., 2002. Monitoring the composition of urban environments based on the vegetation–impervious surface–soil (VIS) model by subpixel analysis

techniques. International Journal of Remote Sensing 23(20), 4131-4153.

Powell, R.L., Roberts, D.A., Dennison, P.E., Hess, L.L., 2007. Sub-pixel mapping of urban land cover using multiple endmember spectral mixture analysis: Manaus, Brazil. Remote Sensing of Environment 106(2), 253-267.

Rashed, T., Weeks, J.R., Stow, D., Fugate, D., 2005. Measuring temporal compositions of urban morphology through spectral mixture analysis: toward a soft approach to change analysis in crowded cities. International Journal of Remote Sensing 26(4), 699-718.

Ridd, M.K., 1995. Exploring a V-I-S (vegetation-impervious surface-soil) model for urban ecosystem analysis through remote sensing: comparative anatomy for cities. International Journal of Remote Sensing 16(12), 2165-2185.

Roberts, D.A., Gardner, M., Church, R., Ustin, S., Scheer, G., Green, R., 1998. Mapping Chaparral in the Santa Monica Mountains Using Multiple Endmember Spectral Mixture Models. Remote Sensing of Environment 65(3), 267-279.

Sabol, D.E., Adams, J.B., Smith, M.O., 1992. Quantitative Subpixel Spectral Detection of Targets in Multispectral Images. Journal of Geophsical Research 97(E2), 2659-2672.

Schueler, T.R., 1994. The Importance of Imperviousness. Watershed Protection Techniques 1(3), 137-140.

Small, C., 2001. Estimation of urban vegetation abundance by spectral mixture analysis. International Journal of Remote Sensing 22(7), 1305-1334.

Small, C., Lu, J.W.T., 2006. Estimation and vicarious validation of urban vegetation abundance by spectral mixture analysis. Remote Sensing of Environment 100(4), 441-456.

Smith, M.O., Johnson, P.E., Adams, J.B., 1985. Quantitative Determination of Mineral Types and Abundances from Reflectance Spectra Using Principal Components Analysis. Journal of Geophysical Research 90(C), 797-804.

Song, C., 2004. Cross-sensor calibration between Ikonos and Landsat ETM+ for spectral mixture analysis. Geoscience and Remote Sensing Letters IEEE 1(4), 272-276.

Song, C., 2005. Spectral mixture analysis for subpixel vegetation fractions in the urban environment: How to incorporate endmember variability? Remote Sensing of Environment 95(2), 248-263.

White, M.D., Greer, K.A., 2006. The effects of watershed urbanization on the stream hydrology and riparian vegetation of Los Peñasquitos Creek, California. Landscape and Urban Planning 74(2), 125-138.

Wu, C., 2004. Normalized spectral mixture analysis for monitoring urban composition using ETM+ imagery. Remote Sensing of Environment 93(4), 480-492.

Wu, C., Murray, A.T., 2003. Estimating impervious surface distribution by spectral mixture analysis. Remote Sensing of Environment 84(4), 493-505.

Xian, G., Crane, M., Su, J., 2007. An analysis of urban development and its environmental impact on the Tampa Bay watershed. Journal of Environmental Management 85(4), 965-976.

Yuan, D., Elvidge, C.D., 1996. Comparison of relative radiometric normalization techniques. ISPRS

Journal of Photogrammetry and Remote Sensing 51(3), 117-126.

Yuan, F., Bauer, M.E., 2007. Comparison of impervious surface area and normalized difference vegetation index as indicators of surface urban heat island effects in Landsat imagery. Remote Sensing of Environment 106(3), 375-386.

**Tab. 1 Comparisons of the ISA estimation accuracy among seven SMA- or NSMA-based models**

| | Slope | Intercept | $r^2$ | RMSE(0-100%) | RMSE(0-40%) | RMSE(60-100%) |
|---|---|---|---|---|---|---|
| Method 1 | 0.7253 | 0.1065 | 0.806 | 0.117 | 0.129 | 0.095 |
| Method 2 | 0.9439 | -0.0258 | 0.906 | 0.091 | 0.079 | 0.107 |
| Method 3 | 0.7207 | 0.1396 | 0.863 | 0.114 | 0.130 | 0.081 |
| Method 4 | 0.8797 | 0.0781 | 0.892 | 0.098 | 0.105 | 0.069 |
| Method 5 | 0.9983 | 0.0019 | 0.962 | 0.052 | 0.045 | 0.060 |
| Method 6 | 0.9357 | 0.0194 | 0.940 | 0.075 | 0.056 | 0.098 |
| Method 7 | 0.6351 | 0.2193 | 0.775 | 0.163 | 0.204 | 0.054 |

Note:

Method 1: 4-endmember SMA model (Wu and Murray, 2003)

Method 2: SMA-based model with LST modification (Lu and Weng, 2006)

Method 3: NSMA (Wu 2004)

Method 4: MESMA with a normalized endmember library (including 3 vegetation, low albedo, high albedo and soil endmembers)

Method 5: PNMESMA in this study

Method 6: NSMA only with the first improvement: pre-screening the pure vegetation pixels

Method 7: NSMA only with the second improvement: applying MESMA

**Table 2 Long-term change of ISA in Lake Kasumigaura Basin with sub-basins**

| Sub-basin Code | Name of Basin | Area($km^2$) | ISA fraction (%) | | | Change Rate (%/y) | | | Predicted ISA fraction (%) | |
|---|---|---|---|---|---|---|---|---|---|---|
| | | | 1987 | 2000 | 2007 | 87-00 period | 00-07 period | 87-07 period | 2012 | 2017 |
| | Lake Kasumigaura Basin (excluding water area) | 1870.2 | 19.9 | 21.8 | 23.7 | 0.1 | 0.3 | 0.2 | 24.6 | 25.5 |
| 1 | Sakura River | 335.5 | 18.1 | 21.4 | 19.2 | 0.3 | -0.3 | 0.1 | 19.5 | 19.8 |
| 2 | Koise River | 222.3 | 11.7 | 12.3 | 11.2 | 0.0 | -0.1 | 0.0 | 11.1 | 11.0 |
| 3 | Ono River | 176.4 | 25.7 | 27.6 | 32.6 | 0.1 | 0.7 | 0.3 | 34.4 | 36.1 |
| 4 | Shintone River | 143.0 | 18.6 | 20.2 | 27.1 | 0.1 | 1.0 | 0.4 | 29.2 | 31.3 |
| 5 | Tomoe River | 129.7 | 18.8 | 22.8 | 23.7 | 0.3 | 0.1 | 0.2 | 24.9 | 26.1 |
| 6 | Sonobe River | 82.0 | 19.3 | 23.2 | 24.4 | 0.3 | 0.2 | 0.3 | 25.6 | 26.9 |
| 7 | Hokota River | 36.6 | 28.8 | 35.6 | 33.6 | 0.5 | -0.3 | 0.2 | 34.9 | 36.1 |
| 8 | Hanamuro River | 31.7 | 36.5 | 37.2 | 41.8 | 0.1 | 0.7 | 0.3 | 43.2 | 44.5 |
| 9 | Ichinose River | 29.9 | 19.7 | 21.5 | 21.2 | 0.1 | 0.0 | 0.1 | 21.6 | 22.0 |
| 10 | Seimei River | 25.0 | 22.9 | 26.8 | 28.9 | 0.3 | 0.3 | 0.3 | 30.4 | 31.9 |
| 11 | Hishiki River | 23.4 | 20.8 | 18.2 | 18.8 | -0.2 | 0.1 | -0.1 | 18.3 | 17.9 |
| 12 | Yamada River | 20.3 | 15.5 | 17.7 | 19.6 | 0.2 | 0.3 | 0.2 | 20.6 | 21.7 |
| 13 | Sakai River | 19.7 | 34.3 | 39.9 | 42.6 | 0.4 | 0.4 | 0.4 | 44.6 | 46.7 |
| 14 | Takeda River | 19.7 | 19.8 | 23.1 | 22.5 | 0.3 | -0.1 | 0.1 | 23.1 | 23.8 |
| 15 | Kajinashi River | 19.0 | 21.0 | 21.6 | 24.2 | 0.0 | 0.4 | 0.2 | 25.0 | 25.8 |
| 16 | Bizen River | 17.9 | 29.8 | 32.1 | 35.2 | 0.2 | 0.4 | 0.3 | 36.5 | 37.9 |
| 17 | Kura River | 16.7 | 15.3 | 16.3 | 18.8 | 0.1 | 0.3 | 0.2 | 19.6 | 20.5 |
| 18 | Yokosu River | 16.4 | 13.2 | 14.7 | 18.5 | 0.1 | 0.5 | 0.3 | 19.8 | 21.2 |
| 19 | Sanno River | 13.0 | 41.0 | 44.7 | 45.7 | 0.3 | 0.1 | 0.2 | 46.9 | 48.1 |
| 20 | Gantsu River | 8.5 | 15.8 | 17.5 | 19.9 | 0.1 | 0.3 | 0.2 | 20.9 | 21.9 |
| 21 | Shin River | 8.2 | 43.8 | 43.3 | 46.2 | 0.0 | 0.4 | 0.1 | 46.8 | 47.4 |
| 22 | Mae River | 6.5 | 18.3 | 14.3 | 18.1 | -0.3 | 0.5 | 0.0 | 18.1 | 18.1 |
| | Residual | 468.9 | 20.5 | 20.8 | 24.8 | 0.0 | 0.6 | 0.2 | 25.9 | 27.0 |

**Figure List**

Fig.1 Location of the study area. The Lake Kasumigaura Basin is located in the eastern part of the Kanto Plain of Japan. The Landsat TM-5 image was acquired on July 24, 1987. A: Lake Kasumigaura; U: test site for high ISA fraction area (including Tsukuba City and Tsuchiura City); R: test site for medium and low ISA fraction area (Tamazukuri); and M: test site for low ISA fraction area (Makabe) around Mt.Tsukuba.

Fig.2 Feature space representation of the first three PC components for the TOA reflectance image and five endmember reflectance spectra identified through the analysis of the feature spaces. A: vegetation A; B: vegetation B; H: high albedo; L: low albedo; and S: soil.

Fig.3 Feature space representation of the first three PC components for the normalized TOA reflectance image and four endmember were found. A: vegetation A; B: vegetation B; I: ISA; and S: soil.

Fig.4 Normalized TOA reflectance spectrum of each endmember used for the new NSMA-based method developed in this study. The standard deviations of the vegetation reflectance were calculated for the pure vegetation pixels.

Fig.5 Flowchart of the PNMESMA method developed in this study. B3: TOA reflectance of vegetation A at band 3; p and q are the thresholds for NDVI and B3.

Fig.6 Results of ISA estimation accuracy assessment for the image acquired on July 24, 1987: (a)

and (b) results of the 4-endmember SMA; (c) and (d) results of the SMA with the refinement using land surface temperature; (e) and (f) results of the NSMA; (g) and (h) results of the MESMA but used NSMA instead of SMA; (i) and (j) results of the PNMESMA developed in this study. The dashed line is 1:1 line and the solid line is the regression line. The number of validation samples is 138.

Fig.7 Additional results of ISA estimation accuracy assessment for the image acquired on July 24, 1987: (a) and (b) results of the NSMA only with the first improvement (i.e. pre-screening the pure vegetation pixels); (c) and (d) results of the NSMA only with the second improvement (i.e. applying the MESMA). The dashed line is 1:1 line and the solid line is the regression line.

Fig.8 Distribution maps of impervious surface area in Lake Kasumigaura Basin. They were produced by the new NSMA-based method developed in this study: (a) 1987; (b) 2000; and (c) 2007.

Fig.9 Twenty two sub-basins included in Lake Kasumigaura Basin. The numbers in the figure correspond with the sub-basin code in Table 2.

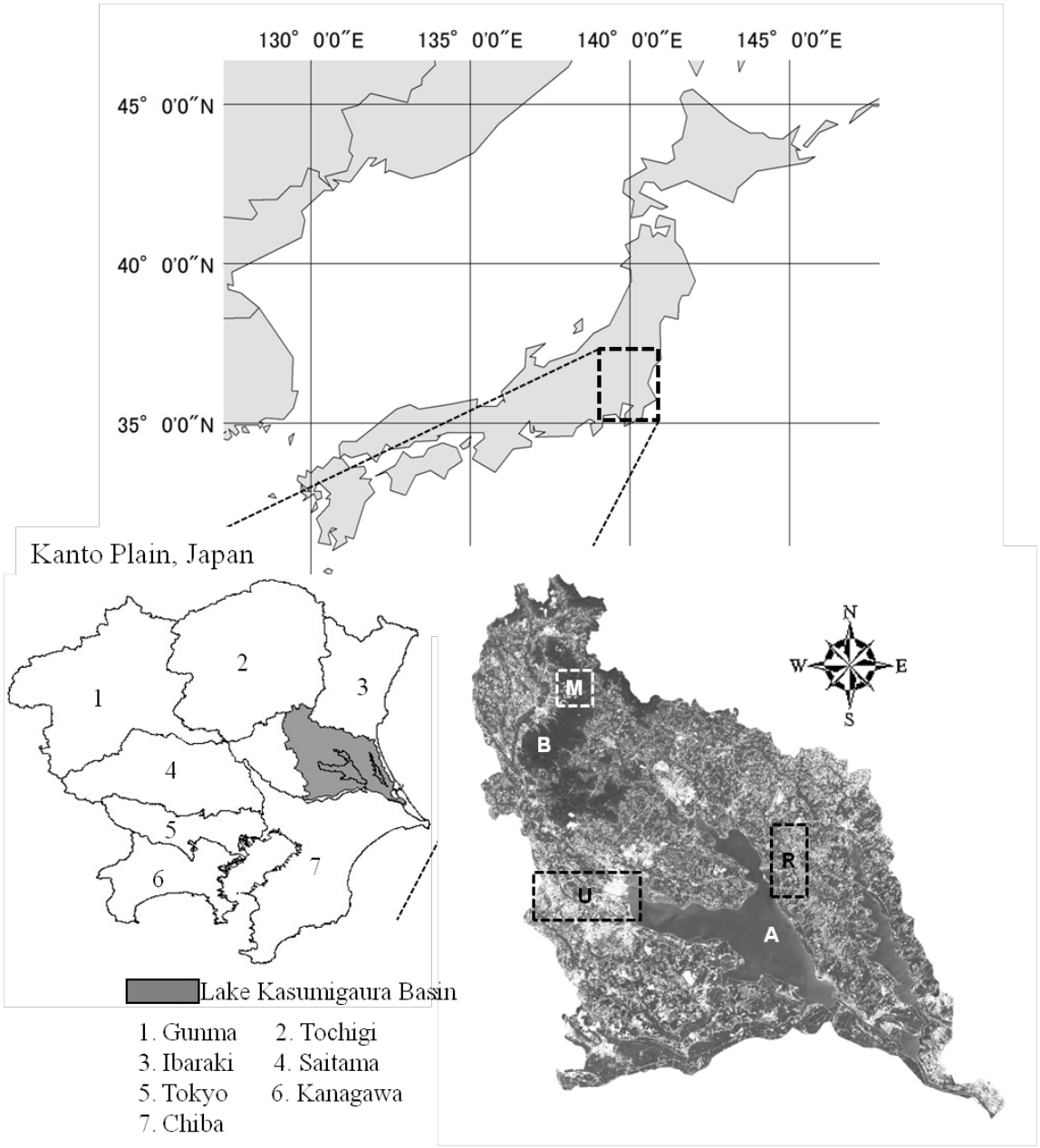
130° 0'0"E
135° 0'0"E
140° 0'0"E
145° 0'0"E
45° 0'0"N
40° 0'0"N
35° 0'0"N
Kanto Plain, Japan
1
2
3
4
5
6
7
Lake Kasumigaura Basin
1. Gunma
2. Tochigi
3. Ibaraki
4. Saitama
5. Tokyo
6. Kanagawa
7. Chiba
N
W
E
S
M
B
R
U
A

**Fig.1**

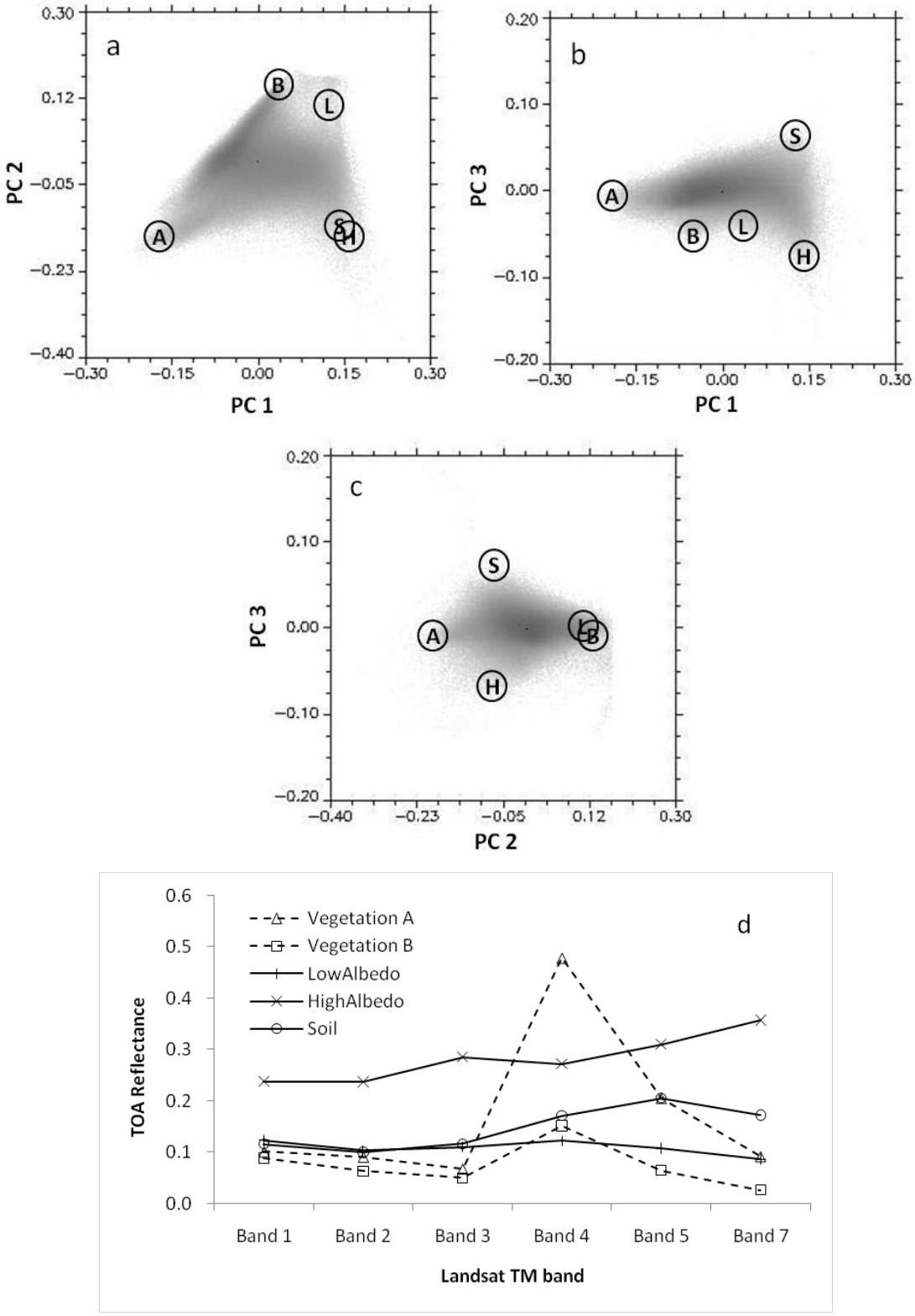
a
PC 2
PC 1
b
PC 3
PC 1
c
PC 3
PC 2
d
Vegetation A
Vegetation B
LowAlbedo
HighAlbedo
Soil
TOA Reflectance
Band 1
Band 2
Band 3
Band 4
Band 5
Band 7
Landsat TM band

**Fig.2**

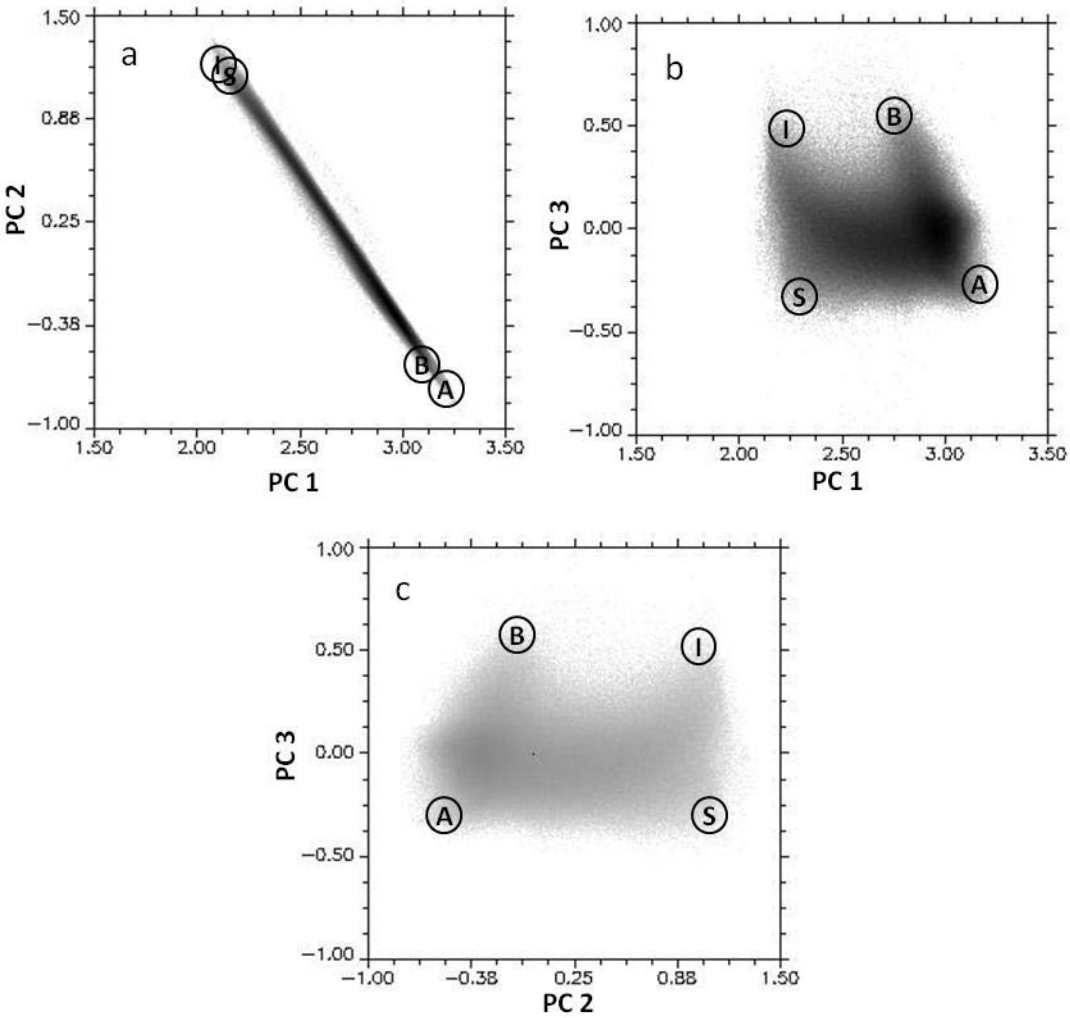
a
I
S
B
A
PC 2
PC 1
1.50
0.88
0.25
−0.38
−1.00
1.50
2.00
2.50
3.00
3.50
b
I
B
S
A
PC 3
PC 1
1.00
0.50
0.00
−0.50
−1.00
1.50
2.00
2.50
3.00
3.50
c
B
I
A
S
PC 3
PC 2
1.00
0.50
0.00
−0.50
−1.00
−1.00
−0.38
0.25
0.88
1.50

**Fig.3**

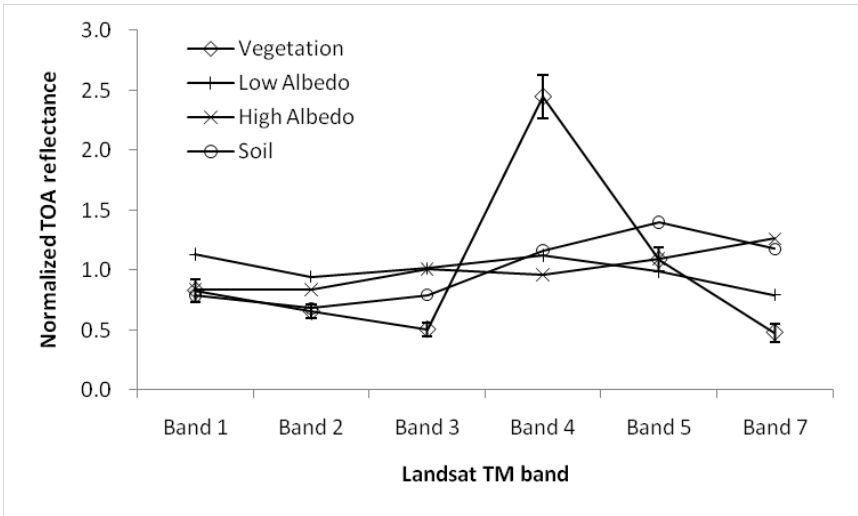
3.0
2.5
2.0
1.5
1.0
0.5
0.0
Normalized TOA reflectance
Vegetation
Low Albedo
High Albedo
Soil
Band 1
Band 2
Band 3
Band 4
Band 5
Band 7
Landsat TM band

**Fig.4**

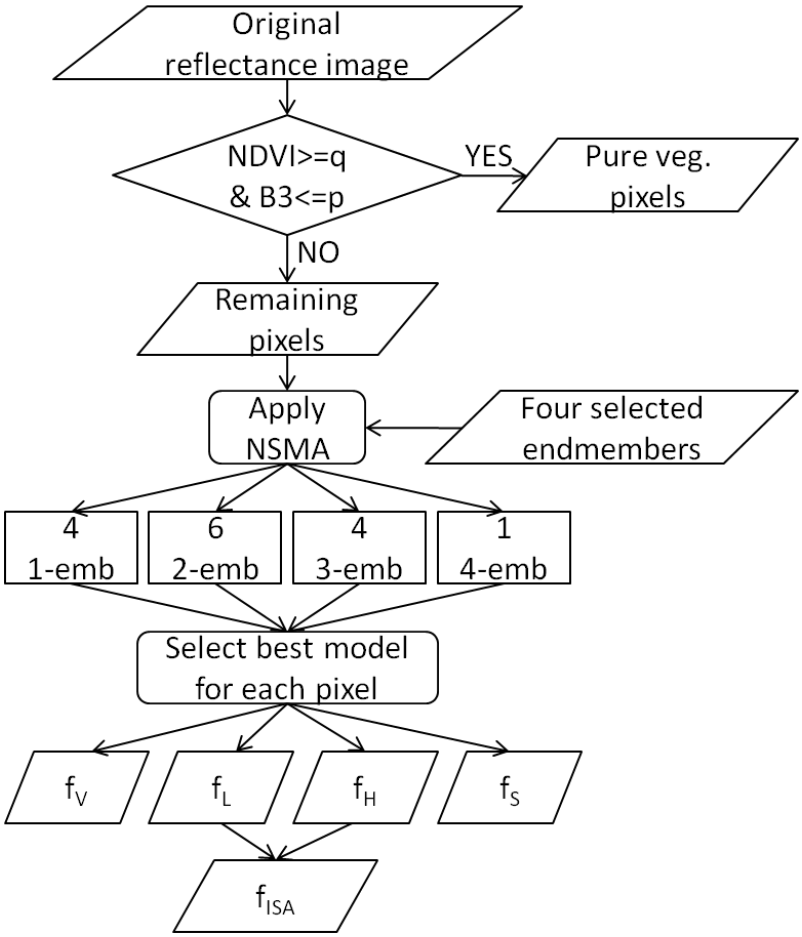
Original reflectance image
NDVI>=q & B3<=p
YES
Pure veg. pixels
NO
Remaining pixels
Apply NSMA
Four selected endmembers
4 1-emb
6 2-emb
4 3-emb
1 4-emb
Select best model for each pixel
$f_V$
$f_L$
$f_H$
$f_S$
$f_{ISA}$

**Fig.5**

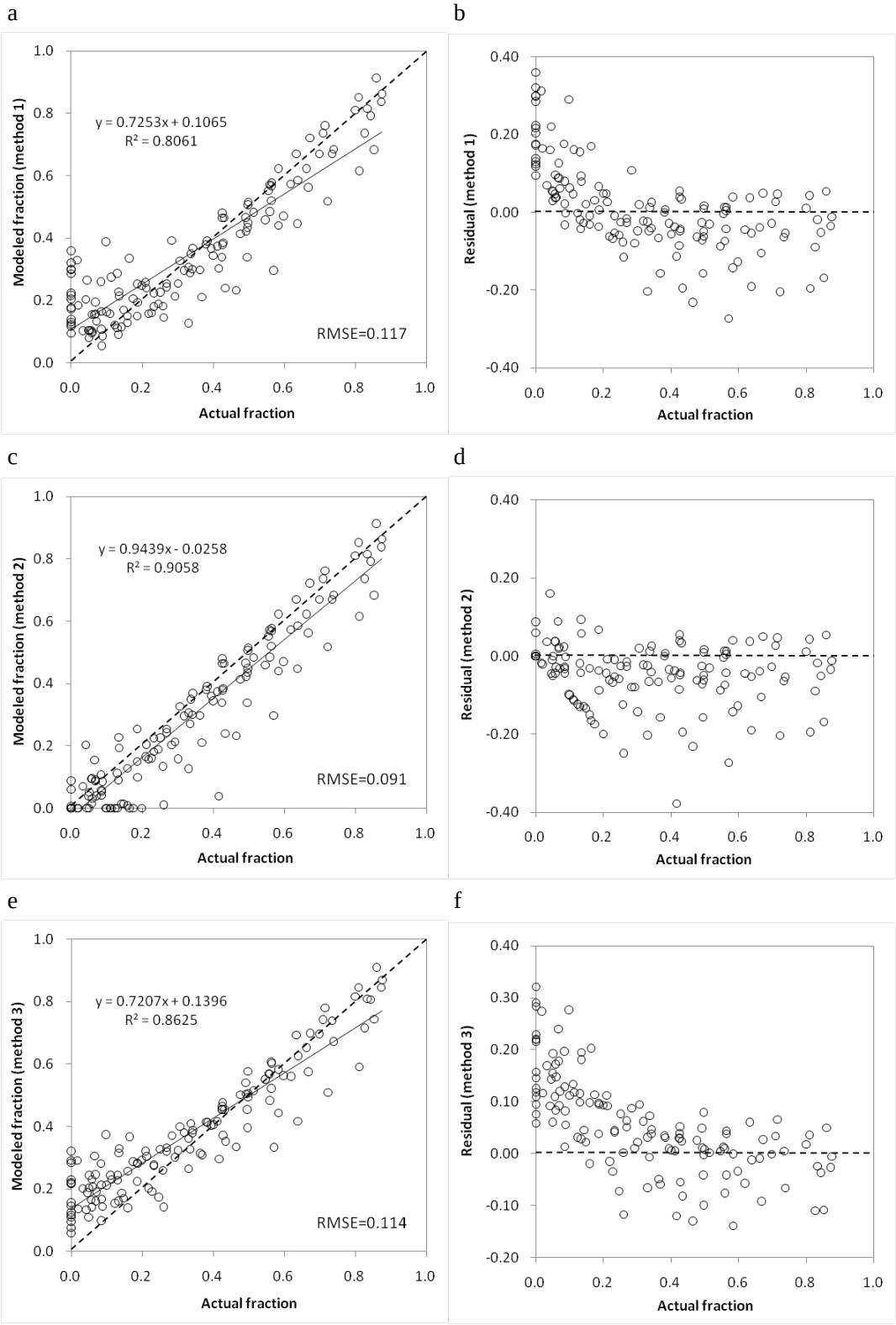
a
b
c
d
e
f
y = 0.7253x + 0.1065
R² = 0.8061
RMSE=0.117
Modeled fraction (method 1)
Residual (method 1)
y = 0.9439x - 0.0258
R² = 0.9058
RMSE=0.091
Modeled fraction (method 2)
Residual (method 2)
y = 0.7207x + 0.1396
R² = 0.8625
RMSE=0.114
Modeled fraction (method 3)
Residual (method 3)
Actual fraction

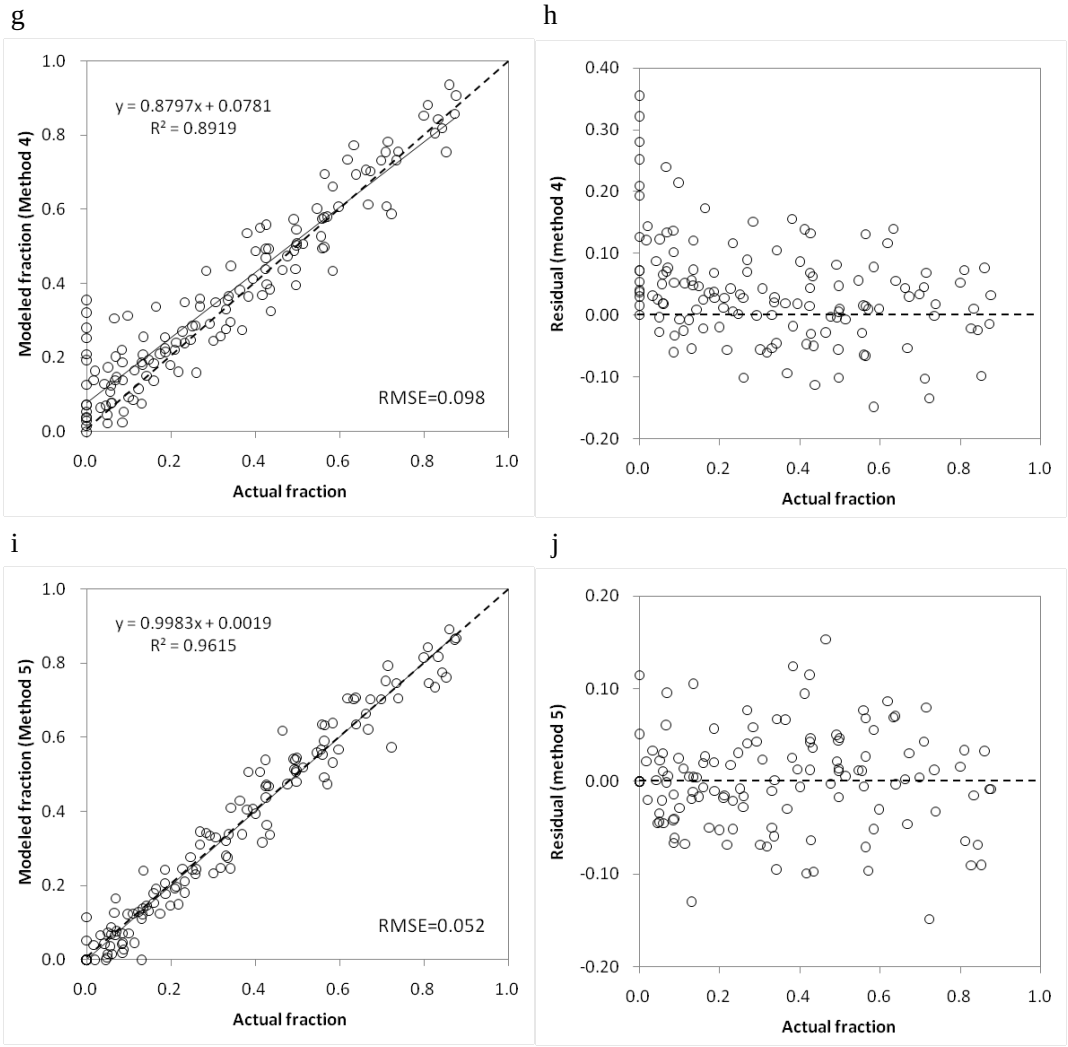
g
h
y = 0.8797x + 0.0781
R² = 0.8919
RMSE=0.098
Modeled fraction (Method 4)
Actual fraction
Residual (method 4)
Actual fraction
i
j
y = 0.9983x + 0.0019
R² = 0.9615
RMSE=0.052
Modeled fraction (Method 5)
Actual fraction
Residual (method 5)
Actual fraction

**Fig.6**

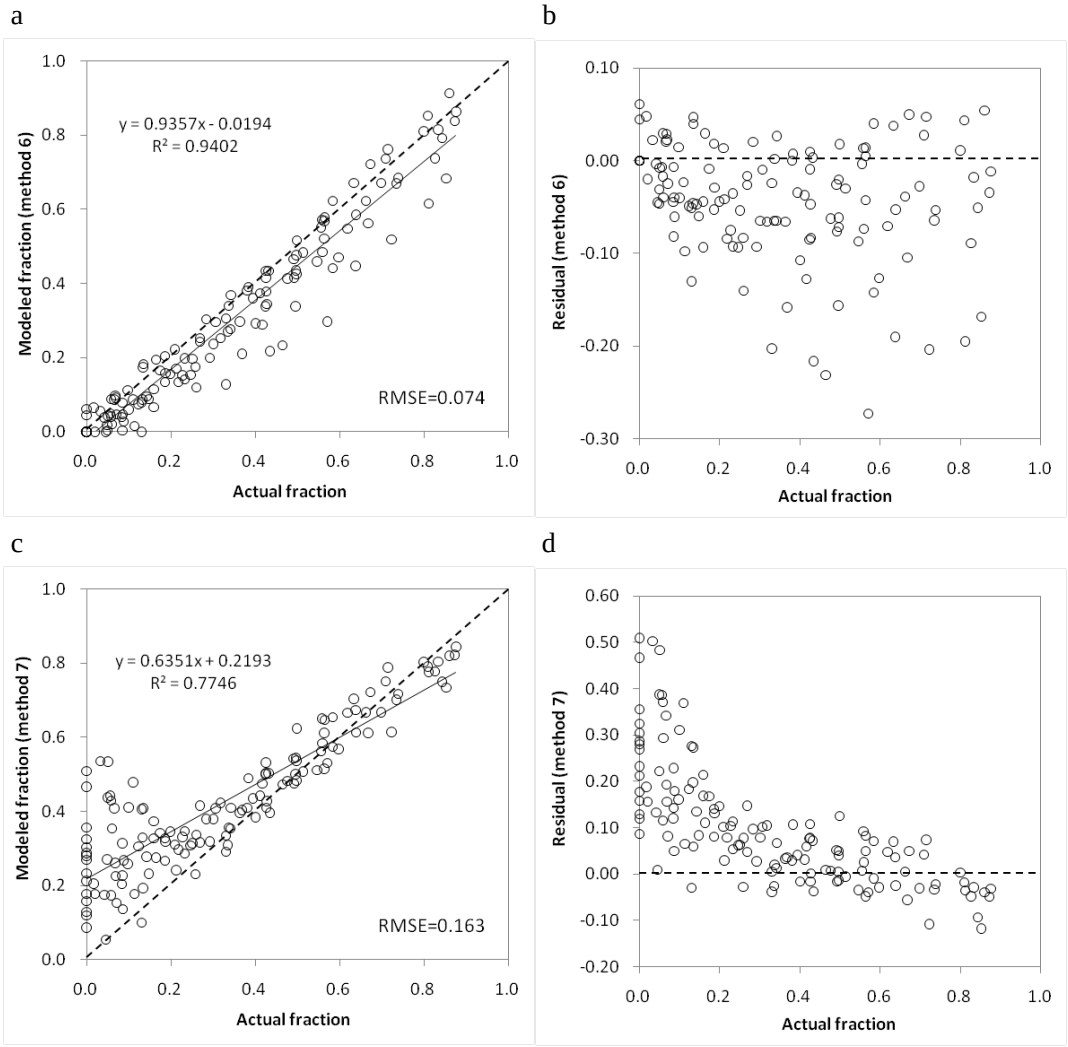
a
b
c
d
y = 0.9357x - 0.0194
R² = 0.9402
RMSE=0.074
Modeled fraction (method 6)
Actual fraction
Residual (method 6)
Actual fraction
y = 0.6351x + 0.2193
R² = 0.7746
RMSE=0.163
Modeled fraction (method 7)
Actual fraction
Residual (method 7)
Actual fraction

**Fig.7**

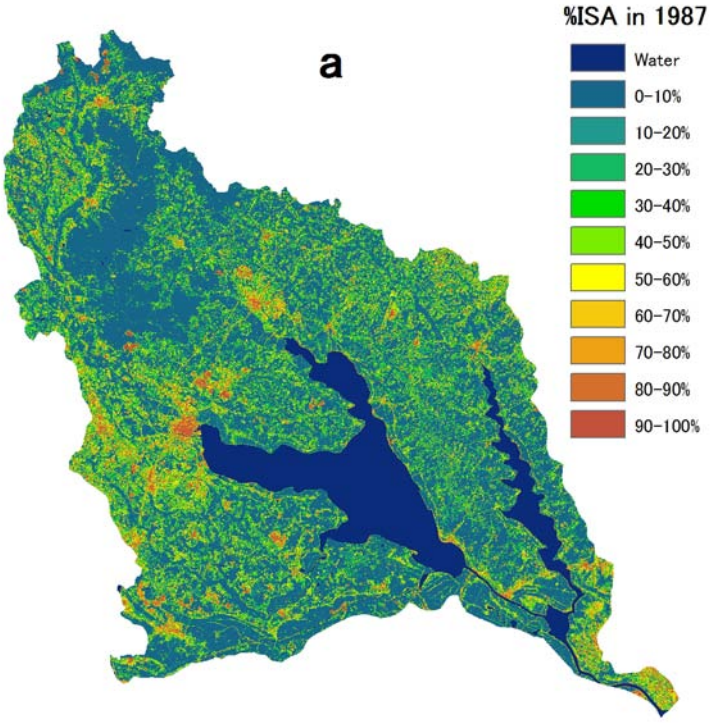
a
%ISA in 1987
Water
0-10%
10-20%
20-30%
30-40%
40-50%
50-60%
60-70%
70-80%
80-90%
90-100%

1

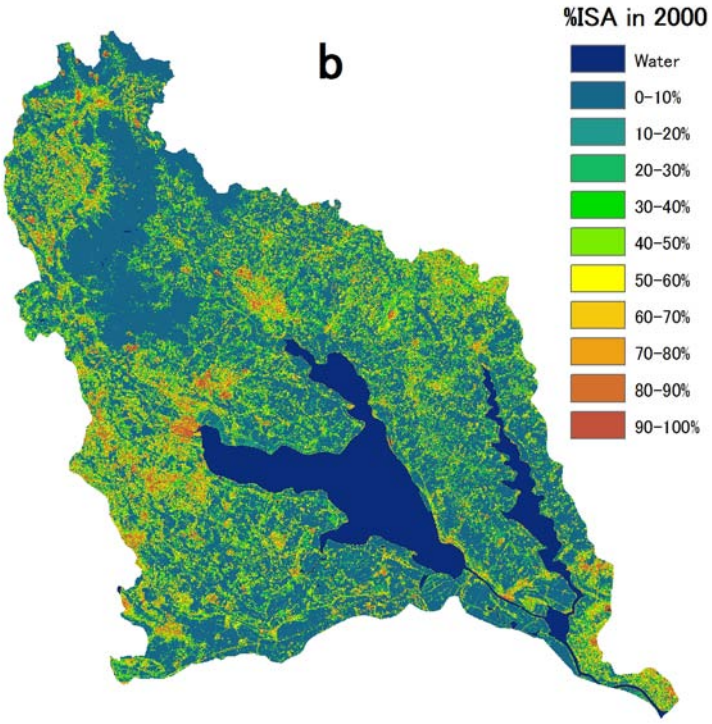
b
%ISA in 2000
Water
0-10%
10-20%
20-30%
30-40%
40-50%
50-60%
60-70%
70-80%
80-90%
90-100%

2

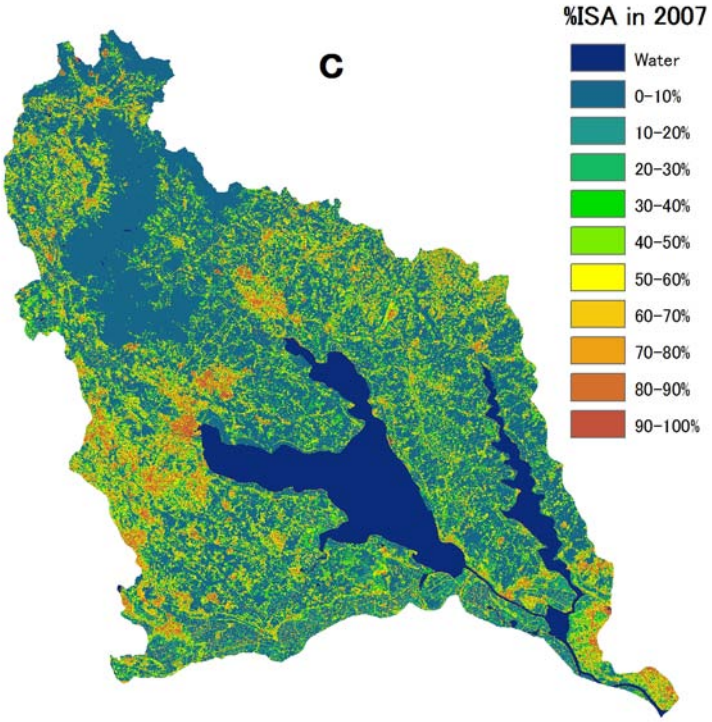
C
%ISA in 2007
Water
0-10%
10-20%
20-30%
30-40%
40-50%
50-60%
60-70%
70-80%
80-90%
90-100%

**Fig.8**

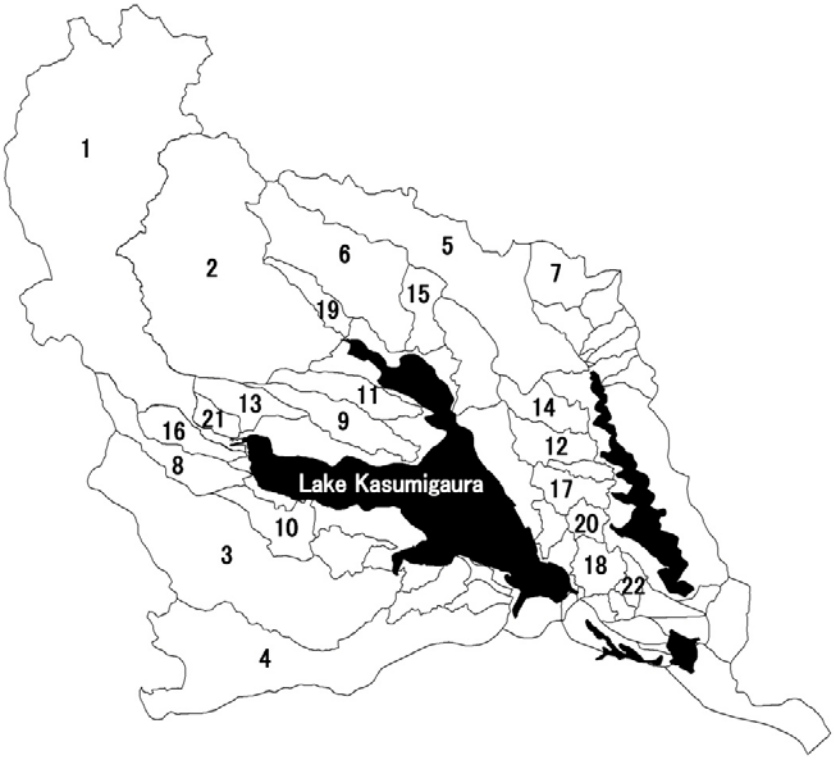
1
2
3
4
5
6
7
8
9
10
11
12
13
14
15
16
17
18
19
20
21
22
Lake Kasumigaura

**Fig.9**